PHYSICAL REVIEW B **69**, 205320 (2004)

Large change in biaxial anisotropy of in-plane hole dispersion in a (110) quantum well under [110] uniaxial stress

Y. Kajikawa, N. Nishimoto, and Y. Higuchi*

Department of Electric and Control Systems Engineering, Interdisciplinary Faculty of Science and Engineering, Shimane University, 1060 Nishi-Kawatsu, Matsue, Shimane 690-8504, Japan

(Received 18 October 2003; revised manuscript received 27 February 2004; published 28 May 2004)

We present a theoretical study of a valence-subband dispersion in a (110)-oriented quantum well (QW) under [110] uniaxial stress. As an example, we present calculated results for a (110) GaAs QW. The 4×4 Luttinger-Kohn $\mathbf{k}\cdot\mathbf{p}$ Hamiltonian in conjunction with the Bir-Pikus strain Hamiltonian is solved within the infinitely high barrier model in order to obtain the in-plane dispersion curves of valence subbands. Then, confinement energies, effective masses along the two orthogonal in-plane directions ([001] and [$\bar{1}$10]), and optical matrix elements for [001] and [$\bar{1}$10] polarized light are obtained at zero in-plane momentum ($k_\parallel=0$) and are plotted as functions of the [110] uniaxial stress. The confinement energies of the first two subbands show anticrossing behavior as functions of the stress. Due to the drastic change in valence-band mixing near the anticrossing, the effective masses of the two subbands show changes in their signs, magnitudes, and in-plane anisotropies. The most outstanding point is the saddle-point character of the first hole subband at $k_\parallel=0$, which appears under the stress corresponding to the anticrossing and under the larger stress. An intimate relation is shown between the biaxial anisotropy in optical matrix elements and that in the hole effective mass. A simple model based on the tight-binding approximation is presented for understanding the intimate relation between them.

DOI: 10.1103/PhysRevB.69.205320 PACS number(s): 73.21.Fg, 73.61.Ey

I. INTRODUCTION

Valence-band engineering in semiconductor quantum wells (QW's) by utilizing strain effects is an important arena for developing high-performance optical and electronic devices. In the theoretical investigations, envelope-function framework, based on the multiband effective-mass theory of the Luttinger-Kohn $\mathbf{k}\cdot\mathbf{p}$ Hamiltonian in the spin $J=3/2$ basis in conjunction with the Bir-Pikus strain Hamiltonian, has been most widely employed to study the valence subband structure in the QW subjected to strain. It is well known that the off-diagonal terms in both the Luttinger-Kohn and the Bir-Pikus Hamiltonians cause valence-band mixing and lead to much more complicated dispersion curves of valence subbands than those of conduction subbands. In addition to the quantum confinement potential and strain field, crystallographic orientation can be another important degree of freedom for tailoring valence-band mixing in the QW. Note that at zero in-plane momentum, mixing between the heavy-hole state with $|J_z|=3/2$ and the light-hole state with $|J_z|=1/2$ is absent in (001) and (111) QW's owing to their high symmetries, whereas it does exist in $(11l)$ QW's ($l\neq1$) due to their lower symmetries even in the absence of strain. Since the symmetries of the QW's remain unchanged by applying the stress perpendicular to the hetero-interfaces, level crossing is allowed between any two confined hole states at zero in-plane momentum in (001) and (111) QW's as a function of the perpendicular stress,[1] whereas the crossing is replaced by anticrossing for two hole states having the same parity in $(11l)$ QW's.[2,3]

Several experimental studies revealed that QW's grown along the $[11l]$ directions show remarkably different optical properties from the conventional (001) QW's. Such a difference comes partially from the lower symmetries of the $(11l)$ QW's than those of the (001) and (111) QW's. Namely, while the square and hexagonal symmetries of the (001) and (111) QW's, respectively, promise isotropic optical property, the rectangular symmetry of $(11l)$ QW's results in biaxial dependence on in-plane polarization. For example, it has been shown both experimentally and theoretically that (110),[4] (112),[5] and (113) (Ref. 6) unstrained QW's exhibit anisotropic dependence of optical transitions on the in-plane linear polarization. Furthermore, theoretical studies suggest that the anisotropy can be modified by changing the extent of mixing among the heavy-hole, light-hole, and spin-orbit split-off states through varying the well width,[7] the barrier height,[8] strain,[9] or electric field applied externally.[10] Especially, it has been predicted that strain-induced anticrossing between the hole energy levels in (110) QW's leads to perfect linearly polarized dependence of the matrix elements for the interband optical transition.[2,9,11]

Biaxial anisotropy is also shown for the valence subband dispersion in $(11l)$ QW's by theoretical studies.[12–20] Analytical expressions have been derived for anisotropic in-plane effective masses of hole subbands in unstained (110) QW's within the infinite-barrier-height model by Shechter *et al.*[21] They found that some subbands in (110) QW's exhibit saddle-point dispersion at zero in-plane momentum.[22] Similarly, Valadares[23] showed theoretically that some subbands in (113) QW's also exhibit saddle-point dispersion. The saddle-point character of some valence subbands in a (113) QW has been evidenced by resonant magnetotunneling spectroscopy on a double-barrier AlAs/GaAs/AlAs resonant tunneling diode structure.[24,25] However, in the unstrained QW's investigated in these studies, the saddle-point dispersion is found only for higher-order subbands having quantum numbers $n>1$.

In the present study, we calculate the valence subband

 ©2004 The American Physical Society

dispersion in a (110)-oriented QW under the uniaxial stress perpendicular to the hetero-interfaces within the four-band effective-mass approximation in the spin $J=3/2$ basis. In Sec. II we briefly describe the calculation method for valence subband dispersion. In Sec. III the calculated results are shown for a (110) GaAs QW under the [110] uniaxial stress. A main result of this work is the finding that the first ($n=1$) subband of hole shows the saddle-point dispersion under adequate stresses. Relation between the anisotropy in optical matrix elements and that in effective masses is discussed in Sec. IV.

II. CALCULATION METHOD

We deal with a semiconductor single QW having a well width of d whose heterointerfaces are parallel to the (110) plane. We use the (110) film coordinate system where the axes are taken so that $x\|[00\bar{1}]$, $y\|[\bar{1}10]$, and $z\|[110]$. We assume the barrier height of the QW is infinite.

According to the four-band effective-mass theory, the valence-band structure near the Γ_8 point of bulk III-V compounds subjected to the strain can be obtained by using the following type of a 4×4 Hamiltonian, which is defined in an orthonormal basis set $\{|J,J_z\rangle\}$ of a cell-periodic wave function at $\mathbf{k}=0$, where $J=\frac{3}{2}$ and $J_z=-\frac{3}{2}, -\frac{1}{2}, \frac{1}{2}, \frac{3}{2}$ designate the total angular momentum and its z components, respectively:

$$H=\begin{pmatrix} L & S & N & 0 \\ S^* & M & 0 & N \\ N^* & 0 & M & -S \\ 0 & N^* & -S^* & L \end{pmatrix} \begin{matrix} |\frac{3}{2},-\frac{3}{2}\rangle \\ |\frac{3}{2},-\frac{1}{2}\rangle \\ |\frac{3}{2},\frac{1}{2}\rangle \\ |\frac{3}{2},\frac{3}{2}\rangle \end{matrix}. \tag{1}$$

Here each matrix element is the sum of the corresponding matrix elements of the Luttinger-Kohn (LK) and the Bir-Pikus (BP) Hamiltonians:

$$L=L_{\mathrm{LK}}(k_x,k_y,k_z)+L_{\mathrm{BP}}, \tag{2a}$$

$$M=M_{\mathrm{LK}}(k_x,k_y,k_z)+M_{\mathrm{BP}}, \tag{2b}$$

$$N=N_{\mathrm{LK}}(k_x,k_y,k_z)+N_{\mathrm{BP}}, \tag{2c}$$

$$S=S_{\mathrm{LK}}(k_x,k_y,k_z)+S_{\mathrm{BP}}. \tag{2d}$$

The expressions for these matrix elements of the Luttinger-Kohn and the Bir-Pikus Hamiltonians in the (110) film coordinate system are given in the Appendix, which are quoted from Ref. 18.

The hole wave function in the QW can be written as

$$\Phi(\mathbf{r})=F_{-3/2}(\mathbf{r})|\tfrac{3}{2},-\tfrac{3}{2}\rangle+F_{-1/2}(\mathbf{r})|\tfrac{3}{2},-\tfrac{1}{2}\rangle+F_{1/2}(\mathbf{r})|\tfrac{3}{2},\tfrac{1}{2}\rangle + F_{3/2}(\mathbf{r})|\tfrac{3}{2},\tfrac{3}{2}\rangle, \tag{3}$$

where

$$\mathbf{F}(\mathbf{r})={}^t[F_{-3/2}(\mathbf{r}),F_{-1/2}(\mathbf{r}),F_{1/2}(\mathbf{r}),F_{3/2}(\mathbf{r})] ={}^t[f_{-3/2}(\mathbf{r}),f_{-1/2}(\mathbf{r}),f_{1/2}(\mathbf{r}),f_{3/2}(\mathbf{r})]\exp[i(k_x x+k_y y)]$$

is the four-component envelope function which satisfies $H\mathbf{F}(\mathbf{r})=E\mathbf{F}(\mathbf{r})$ in the QW $(-d/2<z<d/2)$ and vanishes at the interfaces $(z=\pm d/2)$.

For the confined state in the square QW, $\Phi(\mathbf{r})$ has either of the odd or even parity. For the odd state, the four-component envelope function at $\mathbf{k}_\|=(k_x,k_y)$ can be written in the form,[26]

$$\mathbf{f}(z)=\begin{pmatrix} f_{-3/2}(z) \\ f_{-1/2}(z) \\ f_{1/2}(z) \\ f_{3/2}(z) \end{pmatrix} =A_1\begin{pmatrix} S_1\cos(k_1z) \\ -iL_1\sin(k_1z) \\ 0 \\ iN_1^*\sin(k_1z) \end{pmatrix}+B_1\begin{pmatrix} -N_1\cos(k_1z) \\ 0 \\ L_1\cos(k_1z) \\ iS_1^*\sin(k_1z) \end{pmatrix} +A_2\begin{pmatrix} S_2\cos(k_2z) \\ -iL_2\sin(k_2z) \\ 0 \\ iN_2^*\sin(k_2z) \end{pmatrix}+B_2\begin{pmatrix} -N_2\cos(k_2z) \\ 0 \\ L_2\cos(k_2z) \\ iS_2^*\sin(k_2z) \end{pmatrix}, \tag{4}$$

where

$$L_{j\pm}=L(k_x,k_y,\pm k_j)-E, \tag{5a}$$

$$N_{j\pm}=N(k_x,k_y,\pm k_j), \tag{5b}$$

$$S_{j\pm}=S(k_x,k_y,\pm k_j). \tag{5c}$$

In the above equations, k_j $(j=1, 2)$ denotes the absolute values of the solutions of k_z for the bulk hole dispersion relation

$$E=(L+M)/2\pm[(L-M)^2/4+NN^*+SS^*]^{1/2} \tag{6}$$

in the presence of strain for a given energy and $\mathbf{k}_\|=(k_x,k_y)$. k_1 corresponds to the solution of Eq. (6) with the plus sign, while k_2 to that with the minus one.

In case of the (001) QW problem in which k_z is taken along [001], the plus sign in Eq. (6) (and thus k_1) corresponds to heavy holes (hh) while the minus sign (and thus k_2) to light holes (lh). Explicit forms of the solutions k_j in the [001] direction are given by Eq. (29) in Ref. 1 or by Eqs. (5) and (6) in Ref. 27 for the strained film on the (001) substrate. (However, note that the second term in the right-hand side of Eq. (6) in Ref. 27 should be $C^4k_\|^4/4$ instead of $C^4k_\|^4$.)

For the purpose of solving the (110) QW problem, the solutions k_j in the [110] direction are necessary. Their explicit forms in the absence of strain are given by Eqs. (6) and (8) in Ref. 15. [Note that in Ref. 15 the first term in the right-hand side of Eq. (8) in the expression for b should be $E^2(\gamma_2^2+3\gamma_3^2)$ instead of $E^2(\gamma_2^2+\gamma_3^2)$ and that the values of the coefficients in the expressions for R in Eqs. (3), (4), and (5) are also incorrect.]

In the absent of strain, the plus sign in Eq. (6) (and thus k_1) corresponds to the heavy-hole branch and the minus sign

(and thus k_2) to the light-hole one as in the case of the (001) QW problem. On the other hand, in the presence of strain, the terms "heavy- (light-) hole branch" become meaningless for the (110) QW. Then, we refer to the v1 and v2 branches instead of the heavy- and light-hole branches in the presence of strain, corresponding to k_1 and k_2, respectively. Deriving explicit forms of k_j for the (110) QW in the presence of strain is also straightforward, but the expressions are too long to be written here.

The requirement for the vanishing of $\mathbf{f}(z)$ at $z=\pm d/2$ yields the following equation:

$$\det\begin{bmatrix} S_1c_1 & -N_1c_1 & S_2c_2 & -N_2c_2 \\ -iL_1s_1 & 0 & -iL_2s_2 & 0 \\ 0 & L_1c_1 & 0 & L_2c_2 \\ -iN_1^*s_1 & iS_1^*s_1 & iN_2^*s_2 & iS_2^*s_2 \end{bmatrix}=0, \quad (7)$$

where

$$c_j=\cos(k_jd/2), \quad (8a)$$

$$s_j=\sin(k_jd/2). \quad (8b)$$

For $k_\parallel=0$, Eq. (7) reduces to $\cos(k_1d/2)\cos(k_2d/2)=0$ for the odd state, while $\sin(k_1d/2)\sin(k_2d/2)=0$ must be satisfied for the even state. Thus, $k_1=n\pi/d$ or $k_2=n\pi/d$ must be satisfied at $k_\parallel=0$. Inserting these values for k_1 and k_2 to Eq. (6) gives the nth energy level at $k_\parallel=0$ corresponding to the v1 or v2 branch, respectively. Therefore, hole subbands in the (110) strained QW can be referred to as v1_n or v2_n. For each hole subband, the dispersion curve in the presence of strain can be obtained by solving Eq. (7) for the values of $k_\parallel\neq 0$.

In case of the (001) strained QW, the equation corresponding to Eq. (7) can be reduced to the compact form as is given by Eq. (16) in Ref. 28 or by Eq. (12) in Ref. 29. (Note that in Ref. 28, $\gamma^3k_\parallel k_Hk_L$ in the last term in the right-hand side of Eq. (16) should be replaced by $\gamma^3k_\parallel^2k_Hk_L$ and that the value of the coefficient in the expression for L in Eq. (6) is also incorrect. Note also that, in Ref. 29, $[(P_2+Q_2+S-\varepsilon)(P_2-Q_2-S-\varepsilon)-2R^2]$ in the right-hand side of Eq. (12) should be replaced by $[(P_1+Q_1+S-\varepsilon)(P_2-Q_2-S-\varepsilon)-2R^2]$ and that the values of the coefficients in Eqs. (7) and (9) are also incorrect.) A similar compact form can be obtained for the (110) QW problem in the absence stain, as is given by Eq. (7) in Ref. 21. On the other hand, such a compact form cannot be obtained anymore in case of the (110) QW in the presence of strain. It is, therefore, necessary to solve Eq. (7) directly for calculating the valence subband dispersion in the (110) strained QW.

III. RESULTS OF CALCULATIONS

We consider here a (110)-oriented GaAs QW having a well width of 10 nm under the [110] uniaxial stress. The dispersion curves of valence subbands in a 10-nm (110) GaAs QW in the absence of stress have been calculated by Shechter *et al.*[21] and shown in Fig. 1 of their paper. In order to check our calculated results by comparing them with the results in Ref. 21, the Luttinger parameters for GaAs are taken to be the same as in Ref. 22, while deformation potentials and stiffness constants for GaAs are taken to be the same as in our previous studies.[9,11] Our results precisely reproduce those in Fig. 1 of Ref. 21. As can be seen in Fig. 1 of Ref. 21, the dispersion and hence the effective masses of hole subbands are already anisotropic under zero stress. Especially, the hh_2 subband shows saddle-point dispersion. Effective masses along [001] and $[\bar{1}10]$ at $k_\parallel=0$ may be obtained by the parabolic fit or by utilizing analytic formula of Eqs. (9) and (10) in Ref. 21. [Note that the numerator of the last term in Eq. (10) in Ref. 21 should be $6\gamma_1(\gamma_3^2-\gamma_2^2)$ instead of $6\gamma_1(\gamma_3-\gamma_2)$.]

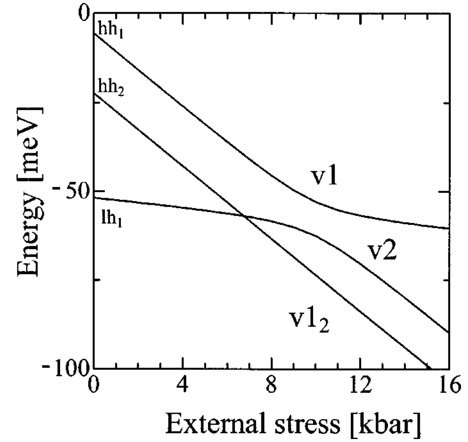

FIG. 1. Energies of the v1, v1_2, and v2 subbands at $k_\parallel=0$ in a 10-nm (110)-oriented GaAs QW relative to the valence-band top of bulk GaAs as functions of the [110] stress.

When applying external stress to the QW, the subband states cannot be categorized to hh or lh anymore due to the valence-band mixing even at $k_\parallel=0$. Therefore, the hole subbands in the QW under stress are designated as v1_n and v2_n instead of hh_n and lh_n (see also Sec. 2 of Appendix B in Ref. 11). For $n=1$, by omitting n, we hereafter denote simply v1 and v2 instead of v1_1 and v2_1, respectively. The energies of the v1, v1_2, and v2 subbands at $k_\parallel=0$ relative to the valence-band top of bulk GaAs are plotted as functions of the [110] uniaxial stresses (X) in Fig. 1. Figures 2(a), 2(b), and 2(c) show the calculated results of the in-plane dispersion curves for the v1, v1_2, and v2 subbands under the [110] uniaxial stresses of 6, 8, and 10 kbar, respectively. The zero of energy in each figure is chosen as the top of the valence band of bulk GaAs under the same uniaxial stress as the QW is subjected to.

The valence-band top of bulk GaAs has the light-hole character under the compressive external uniaxial stress. Since the energy of the v2 subband at $k_\parallel=0$ shifts almost parallel to that of the valence-band top of bulk GaAs as long as the external stress is small, it remains almost constant with respect to the reference point of energy. On the other hand, the energies of the v1 and v1_2 subbands at $k_\parallel=0$ relative to the reference point are lowered with increasing the external stress. As can be seen in Fig. 1, the zone-center energies of the v1_2 and v2 subbands cross at $X\approx 7$ kbar. This indicates that the v1_2 and v2 subbands do not couple at $k_\parallel=0$. This is

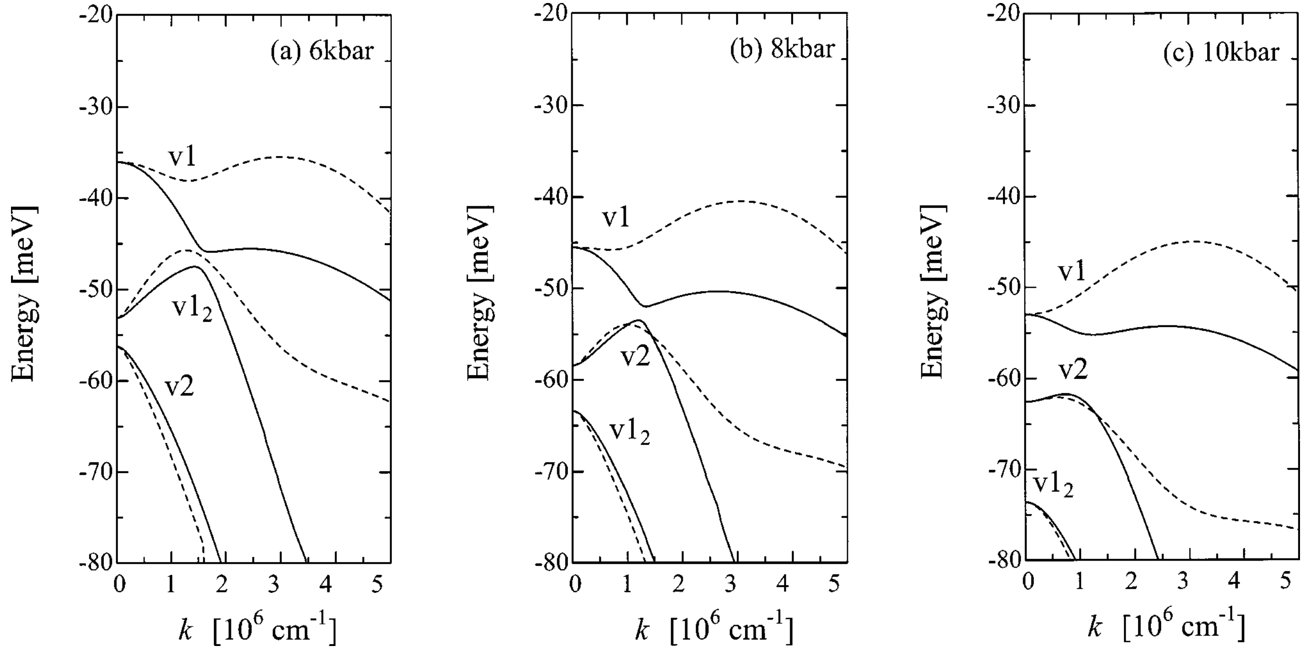

FIG. 2. In-plane dispersion for the v1, $v1_2$, and v2 subbands in a 10-nm (110)-oriented GaAs QW under external stresses along [110] of (a) 6 kbar, (b) 8 kbar, and (c) 10 kbar. Solid curves show the dispersion along $[\bar{1}10]$, while broken ones show that along [001].

owing to the orthogonality between the wave functions having different parities at $k_\parallel = 0$. On the other hand, the $v1_2$ and v2 subbands couple at $k_\parallel \neq 0$ owing to the valence-band mixing, and show repulsive behavior. This repulsion is enhanced with the decrease in energy separation between the $v1_2$ and v2 subbands by increasing the stress to 7 kbar. Owing to the enhanced repulsion, the $v1_2$ subband loses its saddle point at $k_\parallel = 0$, and has a negative (electroniclike) mass along either of [001] and $[\bar{1}10]$ at $X = 6$ kbar, as can be seen in Fig. 2(a).

By applying larger stress than 7 kbar, the order in energy at $k_\parallel = 0$ is reversed between the $v1_2$ and v2 subbands, as shown in Fig. 1. Corresponding to this reversal, the dispersion curves of the v2 subband are plotted over those of the $v1_2$ subband in Fig. 2(b). In spite of this reversal at $k_\parallel = 0$, one can see there that the shapes of the dispersion curves for the two subbands are not changed so much as a whole.

On the other hand, the dispersion curves of the v1 subband change remarkably when the stress is increased beyond 6 kbar. While the dispersion curves of the v1 subband along [001] and $[\bar{1}10]$ are both convex at $k_\parallel = 0$ under the stress of $X = 6$ kbar, the curve along [001] between the two solely becomes almost dispersionless near $k_\parallel = 0$ under the stress of $X = 8$ kbar. For the stress larger than 6 kbar, the top of the v1 subband moves from $k_\parallel = 0$ to $k_\parallel \approx 3 \times 10^{-6}$ cm^{-1} along [001]. Namely, the band gap between the c_1 and the v1 subbands in the QW becomes indirect by applying the external stress larger than 6 kbar. The anisotropy of the v1 subband is enhanced by increasing the stress to $X = 10$ kbar so that the v1 subband has a camel's-back structure with a saddle point at $k_\parallel = 0$ [see Fig. 2(c)].

The inverse effective masses at $k_\parallel = 0$ may be obtained by the parabolic fit to hole subbands up to $k = 5 \times 10^{-5}$ cm^{-1}. The inverse effective masses of the v1 and v2 subbands in the (110) GaAs QW are plotted as a function of the [110] uniaxial stress in Fig. 3(a). Here, we define the signs of hole effective masses so that bulk hole masses in the absence of stress are positive. In the figure, solid curves indicate the inverse masses along $[\bar{1}10]$, while broken ones indicate those along [001].

As can be seen in Fig. 3(a), the inverse mass of the v1 subband along $[\bar{1}10]$ is slightly enlarged at first by applying the stress, and is then drastically diminished when the stress increases from 8 to 12 kbar. For the stress larger than 12 kbar, the $[\bar{1}10]$ inverse mass remains almost constant at the small value. On the other hand, the inverse mass along [001] decreases slowly at first and then steeply to be 0 at $X = 8.5$ kbar; it changes its sign to negative, reaches the negative maximum at $X = 12$ kbar, and shows gradual decrease in absolute value. Note that the zone-center energies of the v1 and the v2 subbands show anticrossing behavior when the stress increases from 8 to 12 kbar, as shown in Fig. 1.

For comparison, the inverse effective masses of the hh_1 and lh_1 subbands at $k_\parallel = 0$ in a 10 nm (001) GaAs QW under the [001] uniaxial stress were calculated, using an analytical expression given by Lee and Vassell.[1] [Note that in the numerator of the last term in the analytical expression of Eq. (34) in Ref. 1, γ_2 should be replaced by γ_3 as has been pointed out by Foreman.[30]] The calculated results of the inverse effective masses are plotted in Fig. 3(b) as a function of the [001] uniaxial stress. In the case of the (001) QW, the order in energy between the hh_1 and lh_1 is reversed for the stress larger than 18 kbar. Namely, the energy levels of hh_1 and lh_1 at the zone center cross each other owing to the high symmetry for this case, in contrast to the anticrossing behavior in the (110) QW case. Comparing Fig. 3(a) with Fig. 3(b), one can see that the effective mass of the v1 subband in the (110) QW shows the heavy-hole character before the level

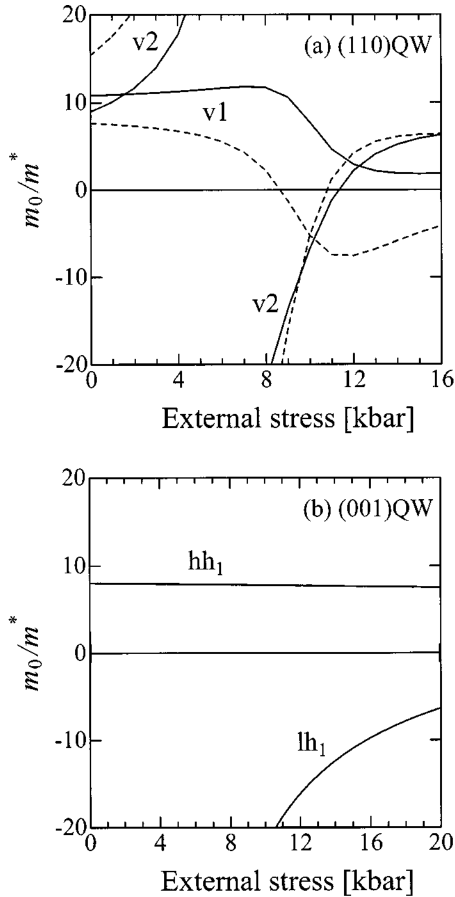

FIG. 3. (a) Inverse effective masses (m_0/m^*) of the v1 and v2 subbands at $k_{\parallel}=0$ in a 10-nm (110)-oriented GaAs QW as a function of the [110] stress. Solid curves represent the inverse masses along [$\bar{1}$10], while broken ones represent those along [001]. (b) Inverse effective masses (m_0/m^*) of the hh_1 and lh_1 subbands at $k_{\parallel}=0$ in a 10-nm (001)-oriented GaAs QW as a function of the [001] stress.

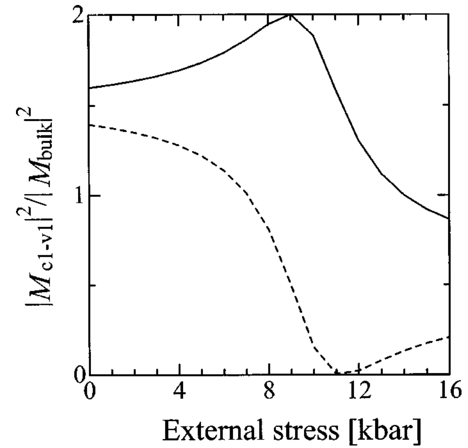

FIG. 4. Squared optical matrix elements of the c_1-v1 transition at $k_{\parallel}=0$ in a 10-nm (110)-oriented GaAs QW for linearly polarized light as functions of the [110] stress. A solid line corresponds to the [$\bar{1}$10] polarization while a broken line to [001]. The values are normalized by the bulk value $|M_b|^2$.

anticrossing and the light-hole one after the anticrossing. On the other hand, the effective mass of the v2 subband seems to take over the heavy-hole character after the anticrossing.

In the anticrossing region, the v1 and v2 states are the strongly mixed states between the $|\frac{3}{2},\pm\frac{3}{2}\rangle$ and $|\frac{3}{2},\mp\frac{1}{2}\rangle$ states even at $k_{\parallel}=0$. As the result, the optical matrix elements between the first conduction subband (c_1) and the v1 (or v2) subband at $k_{\parallel}=0$ show anomalous change in the anisotropy regarding the in-plane polarization of linearly polarized light. According to our previous study,[9] the squared optical matrix elements of the c_1-v1 transition at $k_{\parallel}=0$ for the in-plane polarization are calculated. The results for the (110) GaAs QW are plotted as a function of the [110] uniaxial stress in Fig. 4. In the figure, solid and broken lines represent the squared optical matrix elements for [$\bar{1}$10] and [001] polarized light, respectively, and the ordinates are graduated in the unit of the bulk value $|M_b|^2$ of the squared optical matrix element.

By comparing Fig. 4 with Fig. 3(a), one can see an intimate relation between the anisotropy in optical matrix elements and that in inverse effective masses of the hole subband at the zero in-plane momentum. In the next section we discuss the relation between the anisotropy in optical matrix elements and that in inverse effective masses of the hole subband based on a simplified tight-binding model.

Prior to proceeding to the next section, we mention some experimental implications of the calculated results presented above. If the well or the barrier layer of the (110) QW structure is doped with acceptor impurity to be p type, the holes in the well layer will exhibit anisotropic Hall mobility owing to the anisotropic effective mass of the v1 subband at $k_{\parallel}=0$, as long as the stress is small so that the top of the v1 subband is at $k_{\parallel}=0$. By increasing the stress, the v1 subband exhibits a camel's-back structure, and the top of the v1 subband moves to points with finite k along [001]. The isoenergetic curves around these new top points are ellipses. Then, the Hall mobility exhibits anisotropy, reflecting the anisotropy of the ellipses around the two humps. Thus, the values of the anisotropic mobility will gradually change from the values reflecting the effective masses at $k_{\parallel}=0$ to those reflecting the effective masses at the new top points.

As has been pointed out by Shechter *et al.*,[22] the calculation shows that the saddle-point dispersion of the hh_2 subband at $k_{\parallel}=0$ in the (110) GaAs QW can be found even in the absence of stress. Similarly, the calculation by Valadares[23] shows that some subbands in a (113) GaAs QW exhibit saddle-point dispersion and camel's-back structures in the absence of stress. Using resonant magnetotunneling spectroscopy, Hayden *et al.*[24,25] investigated the in-plane dispersion curves of the hole subbands in a (113) GaAs QW, and revealed that some subbands really have camel's-back structures.

In the unstressed (110) and (113) QW's investigated in the above studies, the saddle-point dispersion is found only for higher order subbands having quantum numbers $n>1$. On the other hand, the saddle-point dispersion is found for the top most valence subband with $n=1$ under the uniaxial stress in the present study. As in the case of the (113) QW, the saddle-point dispersion in the (110) QW, regarding both

the hh_2 subband in the absence of stress and the v1 subband at the presence of the stress, can be examined by resonant magnetotunneling spectroscopy experiments.

Very recently, Takeda *et al.*[31] used angle-resolved photoelectron spectroscopy (ARPES) for observing the dispersion curves of hole subbands in a Si inversion layer. ARPES is a powerful tool for probing directly the electronic structure of solids. Using ARPES, they observed crossings and repulsions of the subbands as well as negative (electronlike) effective masses around $k_{\parallel}=0$, as has been calculated using the triangle potential approximation. This experimental technique can also be used for investigating the unique character of dispersion curves in (110) QW's under the [110] uniaxial stress.

The unusual dispersions of Figs. 2(a)–2(c) may be manifested in infrared-absorption experiments as well as in cyclotron experiments, since the density of states of a two-dimensional saddle point has a logarithmic singularity.[32]

IV. DISCUSSION

In this section, we discuss the relation between the anistropy in optical matrix elements and that in inverse effective masses of hole subbands based on a simplified tight-binding model.

The expansion of the hole wave function $\Phi(\mathbf{r})$ in the $J=\frac{3}{2}$ basis in the envelope-function theory given by Eq. (3) can be transformed into that in the $\{|x\downarrow\rangle,|y\downarrow\rangle,|z\downarrow\rangle,|x\uparrow\rangle,|y\uparrow\rangle,|z\uparrow\rangle\}$ basis as

$$\Phi(\mathbf{r})=G_{x\downarrow}|x\downarrow\rangle+G_{y\downarrow}|y\downarrow\rangle+G_{z\downarrow}|z\downarrow\rangle+G_{x\uparrow}|x\uparrow\rangle+G_{y\uparrow}|y\uparrow\rangle+G_{z\uparrow}|z\uparrow\rangle, \tag{9}$$

where

$$G_{x\downarrow}=\frac{1}{\sqrt{2}}F_{-3/2}-\frac{1}{\sqrt{6}}F_{1/2},$$

$$G_{y\downarrow}=-\frac{i}{\sqrt{2}}F_{-3/2}-\frac{i}{\sqrt{6}}F_{1/2},$$

$$G_{z\downarrow}=\left(\frac{2}{3}\right)^{1/2}F_{-1/2},$$

$$G_{x\uparrow}=-\frac{1}{\sqrt{2}}F_{3/2}+\frac{1}{\sqrt{6}}F_{-1/2},$$

$$G_{y\uparrow}=-\frac{i}{\sqrt{2}}F_{3/2}-\frac{i}{\sqrt{6}}F_{-1/2},$$

$$G_{z\uparrow}=\left(\frac{2}{3}\right)^{1/2}F_{1/2}. \tag{10}$$

For the v1 state at $k_{\parallel}=0$, since $A_1=A_2=B_2=0$ and $S_1=0$, Eq. (4) becomes

$$\mathbf{F}(z)=\mathbf{f}(z)=B_1\cos(\pi z/d)\begin{pmatrix}-N_1\\0\\L_1\\0\end{pmatrix}. \tag{11}$$

Therefore, for the v1 state at $k_{\parallel}=0$, $\mathbf{G}=(G_{x\downarrow},G_{y\downarrow},G_{z\downarrow},G_{x\uparrow},G_{y\uparrow},G_{z\uparrow})$ can be written as

$$\mathbf{G}=\mathbf{C}\sqrt{\frac{2}{d}}\cos\left(\frac{\pi z}{d}\right), \tag{12}$$

where $\mathbf{C}=(C_{x\downarrow},C_{y\downarrow},0,0,0,C_{z\uparrow})$. Thus, the wave function of the v1 state at $k_{\parallel}=0$ is expressed by

$$\Phi^{\mathrm{v1}}_{k_{\parallel}=0}(\mathbf{r})=(C_{x\downarrow}|x\downarrow\rangle+C_{y\downarrow}|y\downarrow\rangle+C_{z\uparrow}|z\uparrow\rangle)\sqrt{\frac{2}{d}}\cos\left(\frac{\pi z}{d}\right). \tag{13}$$

Using the above C_i's, the optical matrix elements for the c_1-v1 transition at $k_{\parallel}=0$ can be expressed as[2,3,9]

$$|M_x|^2=|C_{x\downarrow}|^2P^2,$$

$$|M_y|^2=|C_{y\downarrow}|^2P^2, \tag{14}$$

$$|M_z|^2=|C_{z\uparrow}|^2P^2,$$

where P is the momentum matrix element between the s and p states, $P=\langle s|p_x|x\rangle=\langle s|p_y|y\rangle=\langle s|p_z|z\rangle$. Therefore, the ratio of the squared optical matrix element $|M_x|^2:|M_y|^2:|M_z|^2$ directly represents the ratio of existence probability among the $|x\rangle$, $|y\rangle$, and $|z\rangle$ states.

The $|x\rangle$, $|y\rangle$, and $|z\rangle$ states can be approximately expressed by the linear combination of atomic orbitals (LCAO). For example, the $|x\rangle$ state in a III-V compound semiconductor can be written as

$$\begin{aligned}|x\rangle&\approx\sum_i\left[a\phi^{\mathrm{III}}_{p_x}(\mathbf{r}-\mathbf{R}^{\mathrm{III}}_i)+b\phi^{\mathrm{V}}_{p_x}(\mathbf{r}-\mathbf{R}^{\mathrm{V}}_i)\right]\\&=\sum_i\left[a\frac{x-X^{\mathrm{III}}_i}{|\mathbf{r}-\mathbf{R}^{\mathrm{III}}_i|}\rho^{\mathrm{III}}(|\mathbf{r}-\mathbf{R}^{\mathrm{III}}_i|)+b\frac{x-X^{\mathrm{V}}_i}{|\mathbf{r}-\mathbf{R}^{\mathrm{V}}_i|}\rho^{\mathrm{V}}(|\mathbf{r}-\mathbf{R}^{\mathrm{V}}_i|)\right],\end{aligned} \tag{15}$$

where $\mathbf{R}^{\mathrm{III}}_i=(X^{\mathrm{III}}_i,Y^{\mathrm{III}}_i,Z^{\mathrm{III}}_i)$ and $\mathbf{R}^{\mathrm{V}}_i=(X^{\mathrm{V}}_i,Y^{\mathrm{V}}_i,Z^{\mathrm{V}}_i)$ represent the position vectors of the lattice sites of the group III and V sublattices, respectively, and $\phi^{\mathrm{III(V)}}_{p_x}$ represents the wave function of the p_x orbitals of an isolated group III(V) atom. In the (110) film coordinate system used here, $\Delta\mathbf{R}^{\mathrm{III\text{-}V}}=\mathbf{R}^{\mathrm{III}}_i-\mathbf{R}^{\mathrm{V}}_i=(1/4,0,-\sqrt{2}/4)a_0$, where a_0 is the lattice constant of the cubic lattice of the III-V compound. While $a=b$ stands for elemental semiconductors with the diamond-type structure, $0<a<b$ stands for III-V zinc-blende-type semiconductors. [See Eq. (5.27) in Ref. 33]

The wave function of the v1 state at $k_{\parallel}=0$ given by Eq. (13) can approximately be expressed by LCAO as

$$\Phi^{\mathrm{v1}}_{k_\parallel=0}(\mathbf{r}) \approx \sqrt{\frac{2}{d}}\cos\left(\frac{\pi z}{d}\right)\sum_i \cos\left(\frac{\pi Z_i}{d}\right)u_{\mathrm{v1}}(\mathbf{r}-\mathbf{R}_i), \tag{16}$$

where

$$u_{\mathrm{v1}}(\mathbf{r}-\mathbf{R}_i) = a u^{\mathrm{III}}_{\mathrm{v1}}(\mathbf{r}-\mathbf{R}^{\mathrm{III}}_i) + b u^{\mathrm{V}}_{\mathrm{v1}}(\mathbf{r}-\mathbf{R}^{\mathrm{V}}_i) \tag{17}$$

with

$$u^{\mathrm{III(V)}}_{\mathrm{v1}}(\mathbf{r}-\mathbf{R}^{\mathrm{III(V)}}_i) = C_{x\downarrow}\phi^{\mathrm{III(V)}}_{p_x}(\mathbf{r}-\mathbf{R}^{\mathrm{III(V)}}_i)|\downarrow\rangle + C_{y\downarrow}\phi^{\mathrm{III(V)}}_{p_y}(\mathbf{r}-\mathbf{R}^{\mathrm{III(V)}}_i)|\downarrow\rangle + C_{z\uparrow}\phi^{\mathrm{III(V)}}_{p_z}(\mathbf{r}-\mathbf{R}^{\mathrm{III(V)}}_i)|\uparrow\rangle \tag{18}$$

and $\mathbf{R}_i = (X_i, Y_i, Z_i) = (\mathbf{R}^{\mathrm{III}}_i + \mathbf{R}^{\mathrm{III}}_i)/2$. $u_{\mathrm{v1}}(\mathbf{r}-\mathbf{R}_i)$ can be rewritten as

$$u_{\mathrm{v1}}(\mathbf{r}-\mathbf{R}_i) = C_{x\downarrow}\phi_{p_x}(\mathbf{r}-\mathbf{R}_i)|\downarrow\rangle + C_{y\downarrow}\phi_{p_y}(\mathbf{r}-\mathbf{R}_i)|\downarrow\rangle + C_{z\uparrow}\phi_{p_z}(\mathbf{r}-\mathbf{R}_i)|\uparrow\rangle, \tag{19}$$

where

$$\phi_{p_\alpha}(\mathbf{r}) = a\phi^{\mathrm{III}}_{p_\alpha}(\mathbf{r}-\mathbf{R}^{\mathrm{III}}_0) + b\phi^{\mathrm{V}}_{p_\alpha}(\mathbf{r}-\mathbf{R}^{\mathrm{V}}_0) \quad (\alpha = x,y,z). \tag{20}$$

In the tight-binding approximation, the wave function at a small $\mathbf{k}_\parallel$ can be written as

$$\Phi^{\mathrm{v1}}_{\mathbf{k}_\parallel}(\mathbf{r}) \approx \sqrt{\frac{2}{d}}\cos(k_1 z)\sum_i \cos(k_1 Z_i)\exp(i\mathbf{k}_\parallel\cdot\mathbf{R}_i) \times u_{\mathrm{v1}}(\mathbf{r}-\mathbf{R}_i). \tag{21}$$

This corresponds to neglecting terms proportional to either $\sin(k_1 z)$, $\sin(k_2 z)$, or $\cos(k_2 z)$, while leaving the terms proportional to $\cos(k_1 z)$ in Eq. (4).

The Hamiltonian in the crystal can be written as

$$H = -\frac{\hbar^2}{2m_0}\nabla^2 + V(\mathbf{r}), \tag{22}$$

where $V(\mathbf{r})$ represents the periodic potential for the crystal. The expectation value of this Hamiltonian for the wave function given by Eq. (19) yields the following energy dispersion:

$$E(\mathbf{k}_\parallel) = E_1 - \sum_i t(\mathbf{R}_i)\cos(k_1 Z_i)e^{i\mathbf{k}_\parallel\cdot\mathbf{R}_i}, \tag{23}$$

where $t(\mathbf{R}_i)$ is the transfer integral defined by

$$t(\mathbf{R}_i) = -\int u_{\mathrm{v1}}(\mathbf{r})\Delta V(\mathbf{r})u_{\mathrm{v1}}(\mathbf{r}-\mathbf{R}_i)d\mathbf{r}, \tag{24}$$

with

$$\Delta V(\mathbf{r}) = V(\mathbf{r}) - U^{\mathrm{III}}(\mathbf{r}+\Delta\mathbf{R}^{\text{III-V}}/2) - U^{\mathrm{V}}(\mathbf{r}-\Delta\mathbf{R}^{\text{III-V}}/2). \tag{25}$$

Here, $U^{\mathrm{III}}(\mathbf{r})$ and $U^{\mathrm{V}}(\mathbf{r})$ represent the potentials for the isolated group III and V atoms, respectively. The insertion of Eq. (19) into Eq. (24) yields

$$t(\mathbf{R}_i) = |C_{x\downarrow}|^2 t_{xx}(\mathbf{R}_i) + C^*_{x\downarrow}C_{y\downarrow}t_{xy}(\mathbf{R}_i) + C_{x\downarrow}C^*_{y\downarrow}t_{yx}(\mathbf{R}_i) + |C_{y\downarrow}|^2 t_{yy}(\mathbf{R}_i) + |C_{z\uparrow}|^2 t_{zz}(\mathbf{R}_i), \tag{26}$$

where

$$t_{\alpha\beta}(\mathbf{R}_i) = -\int \phi_{p_\alpha}(\mathbf{r})\Delta V(\mathbf{r})\phi_{p_\beta}(\mathbf{r}-\mathbf{R}_i)d\mathbf{r} \quad (\alpha,\beta = x,y,z). \tag{27}$$

Hereafter we consider the transfer integrals between the nearest-neighbor lattice sites only. The position vectors of the 12 nearest-neighbor lattice sites in the fcc lattice are written in the (110) film coordinate system used here as

$$\mathbf{R}_{\pm x\pm y\pm z} = \left(\pm\frac{1}{2}, \quad \pm\frac{1}{2\sqrt{2}}, \quad \pm\frac{1}{2\sqrt{2}}\right)a_0, \tag{28a}$$

$$\mathbf{R}_{\pm 2y} = \left(0, \quad \pm\frac{1}{\sqrt{2}}, \quad 0\right)a_0, \tag{28b}$$

$$\mathbf{R}_{\pm 2z} = \left(0, \quad 0, \quad \pm\frac{1}{\sqrt{2}}\right)a_0. \tag{28c}$$

Then, the dispersion given by Eq. (23) yields following in-plane effective masses at $k_\parallel = 0$:

$$\frac{1}{m^*_x} = -\frac{2a_0}{\hbar^2}t(\mathbf{R}_{x+y+z}), \tag{29a}$$

$$\frac{1}{m^*_y} = -\frac{2a_0}{\hbar^2}[t(\mathbf{R}_{x+y+z}) + t(\mathbf{R}_{2y})] = \frac{1}{2}\frac{1}{m^*_x} - \frac{a_0}{\hbar^2}t(\mathbf{R}_{2y}). \tag{29b}$$

Here, we assume that $t_{xy}(\mathbf{R}_i)$ and $t_{yx}(\mathbf{R}_i)$ can be neglected in Eq. (26). This assumption can be justified when $a \ll b$ stands in Eq. (15). In this case, one may neglect transfer integrals containing the group III atoms, and may consider only the transfer integrals between the group V atoms. Among the latter transfer integrals, those involving the cross terms of $\phi^{\mathrm{V}}_{p_x}(\mathbf{r})\Delta V(\mathbf{r})\phi^{\mathrm{V}}_{p_y}(\mathbf{r}-\mathbf{R}_i)$ are considered to be small in comparison with those involving $\phi^{\mathrm{V}}_{p_\alpha}(\mathbf{r})\Delta V(\mathbf{r})\phi^{\mathrm{V}}_{p_\alpha}(\mathbf{r}-\mathbf{R}_i)$ $(\alpha = x,y,z)$. Furthermore, using Eq. (14) and the fact that $t_{yy}(\mathbf{R}_{x+y+z}) = t_{zz}(\mathbf{R}_{x+y+z})$, Eqs. (29a) and (29b) can be rewritten as

$$\frac{1}{m^*_x} \approx -\frac{2a_0^2}{\hbar^2}\left[t_{yy}(\mathbf{R}_{x+y+z}) + \frac{|M_x|^2}{P^2}\{t_{xx}(\mathbf{R}_{x+y+z}) - t_{yy}(\mathbf{R}_{x+y+z})\}\right], \tag{30a}$$

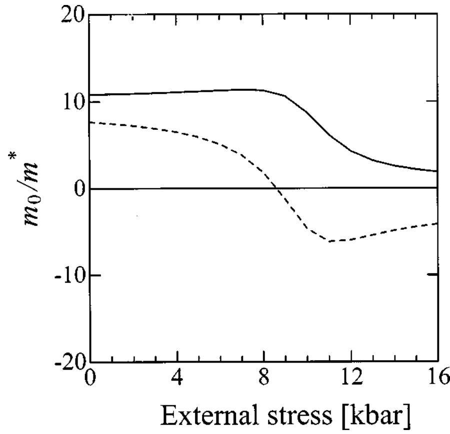

FIG. 5. Fitted results of the inverse effective masses (m_0/m^*) of the v1 subband at $k_\parallel=0$ in a 10-nm (110)-oriented GaAs QW as a function of the [110] stress using analytical expressions of Eq. (30a) for the inverse mass along [001] (indicated by a broken curve) and (30b) for the inverse mass along $[\bar{1}10]$ (indicated by a solid curve).

$$\frac{1}{m_y^*}\approx\frac{1}{2m_x^*}-\frac{a_0^2}{\hbar^2}\left[t_{zz}(\mathbf{R}_{2y})+\frac{|M_x|^2}{P^2}\{t_{xx}(\mathbf{R}_{2y})-t_{zz}(\mathbf{R}_{2y})\}+\frac{|M_y|^2}{P^2}\{t_{yy}(\mathbf{R}_{2y})-t_{zz}(\mathbf{R}_{2y})\}\right]. \tag{30b}$$

These expressions indicate that the change in the optical matrix elements is accompanied with that in the inverse effective masses.

We can fit the curves obtained using analytical expressions of Eqs. (30a) and (30b) to the numerically obtained results shown in Fig. 3(a) by adjusting the transfer integrals as fitting parameters. First, we can estimate the values of $(2a_0^2/\hbar^2)t_{xx}(\mathbf{R}_{x+y+z})$ and $(2a_0^2/\hbar^2)t_{yy}(\mathbf{R}_{x+y+z})$ for the GaAs QW by fitting the results for $1/m_x^*$ shown in Fig. 3(a) using Eq. (30a) with the calculated values of $|M_x|^2/P^2$. Next, we can estimate the values of $(2a_0^2/\hbar^2)t_{xx}(\mathbf{R}_{2y})$, $(2a_0^2/\hbar^2)t_{yy}(\mathbf{R}_{2y})$, and $(2a_0^2/\hbar^2)t_{zz}(\mathbf{R}_{2y})$ by fitting the results for $1/m_y^*$ using Eq. (30b) with the calculated values of the squared optical matrix elements shown in Fig. 4. The fitted curves of the inverse effective masses for the v1 subband in the GaAs QW obtained using Eqs. (30a) and (30b) together with those adjusted parameters are shown in Fig. 5. The curves in Fig. 5 well reproduce those for the inverse effective masses of the v1 subbands in Fig. 3(a). The excellent reproduction suggests the validity of the simplified LCAO model presented above.

V. SUMMARY

We have calculated the valence-subband dispersion for a (110) GaAs QW under the [110] uniaxial stress within the four-band envelope-function model. We have shown that the dispersion curves of the first two (v1 and v2) subbands drastically change when their energies at zero in-plane momentum show anticrossing as a function of the stress. As the results of this change, the signs, the magnitudes, and the anisotropies of the hole effective masses for the v1 and v2 subbands at zero in-plane momentum have been shown to change. Especially, it has been shown that the biaxial anisotropy in the in-plane mass of the v1 subband, which already exists at zero stress, is enhanced by applying the uniaxial stress. This enlarged anisotropy leads to a saddle-point character at $k_\parallel=0$ for the v1 subband. The comparison between the calculated results of the hole effective masses and those of the optical matrix elements showed an intimate relation between them. The relation between the optical matrix elements and the hole effective masses has been explained by a simple LCAO model.

APPENDIX: MATRIX ELEMENTS OF THE HAMILTONIAN

Here we give the expressions for the matrix elements of the Luttinger-Kohn and the Bir-Pikus Hamiltonians in the (110) film coordinate system, which appear in Eqs. (2a)–(2d). For Luttinger parameters we define the linear combinations

$$\gamma_{np}=(n\gamma_3+p\gamma_2)/(n+p), \tag{A1a}$$

$$\bar{\gamma}=(\gamma_3+\gamma_2)/2, \tag{A1b}$$

$$\gamma_\delta=(\gamma_3-\gamma_2)/2. \tag{A1c}$$

The diagonal elements of the Luttinger-Kohn Hamiltonian are given by

$$L_{\rm LK}=P_{\rm LK}+Q_{\rm LK}, \tag{A2a}$$

$$M_{\rm LK}=P_{\rm LK}-Q_{\rm LK}, \tag{A2b}$$

where

$$P_{\rm LK}=\frac{\hbar^2}{2m_0}\gamma_1(k_x^2+k_y^2+k_z^2), \tag{A3a}$$

$$Q_{\rm LK}=\frac{\hbar^2}{2m_0}\left[\gamma_{31}(k_x^2+k_y^2-2k_z^2)-\frac{3}{2}\gamma_\delta(k_x^2-k_y^2)\right]. \tag{A3b}$$

The nondiagonal elements of the Luttinger-Kohn Hamiltonian are given by

$$N_{\rm LK}=\frac{\hbar^2}{m_0}\left[-\frac{\sqrt{3}}{2}\gamma_{53}k_-^2+\frac{\sqrt{3}}{4}\gamma_\delta\left(k_\parallel^2-2k_z^2-\frac{3}{2}k_+^2\right)\right], \tag{A4a}$$

$$S_{\rm LK}=\frac{\hbar^2}{m_0}[\sqrt{3}k_z(\bar{\gamma}k_-+\gamma_\delta k_+)], \tag{A4b}$$

where $k_\parallel^2=k_x^2+k_y^2$, $k_\pm=k_x\pm ik_y$.

For deformation potentials we define

$$\beta_1=-2a=2D_d, \tag{A5a}$$

$$\beta_2=b=\tfrac{2}{3}D_u, \tag{A5b}$$

$$\beta_3=d/\sqrt{3}=\tfrac{2}{3}D_u' \tag{A5c}$$

and the linear combinations

$$\beta_{np}=(n\beta_3+p\beta_2)/(n+p), \tag{A6a}$$

$$\beta_{\delta}=(\beta_3-\beta_2)/2. \tag{A6b}$$

The diagonal elements of the Bir-Pikus Hamiltonian are given by

$$L_{\mathrm{BP}}=P_{\mathrm{BP}}+Q_{\mathrm{BP}}, \tag{A7a}$$

$$M_{\mathrm{BP}}=P_{\mathrm{BP}}-Q_{\mathrm{BP}}, \tag{A7b}$$

where

$$P_{\mathrm{BP}}=\tfrac{1}{2}\beta_1(\varepsilon_{xx}+\varepsilon_{yy}+\varepsilon_{zz}), \tag{A8a}$$

$$Q_{\mathrm{BP}}=\tfrac{1}{2}\beta_{31}(\varepsilon_{xx}+\varepsilon_{yy}-2\varepsilon_{zz})-\tfrac{3}{4}\beta_{\delta}(\varepsilon_{xx}-\varepsilon_{yy}). \tag{A8b}$$

The nondiagonal elements of the Bir-Pikus Hamiltonian are given by

$$N_{\mathrm{BP}}=-\frac{\sqrt{3}}{2}\beta_{53}(\varepsilon_{xx}-\varepsilon_{yy})+\frac{\sqrt{3}}{2}\beta_{\delta}(\varepsilon_{xx}-\varepsilon_{zz}), \tag{A9a}$$

$$S_{\mathrm{BP}}=0. \tag{A9b}$$

Under the [110] uniaxial stress X, the components of the strain tensor are given by

$$\varepsilon_{xx}=-S_{12}X, \tag{A10a}$$

$$\varepsilon_{yy}=-\tfrac{1}{2}(S_{11}+S_{12}-S_{44}/2)X, \tag{A10b}$$

$$\varepsilon_{zz}=-\tfrac{1}{2}(S_{11}+S_{12}+S_{44}/2)X, \tag{A10c}$$

where S_{ij} are elastic compliance constants.

*Present address: Department of Electronics, Graduate School of Engineering, Nagoya University, Chikusa-ku, Nagoya City, Aichi 464-8603, Japan.

[1] J. Lee and M. O. Vassell, Phys. Rev. B **37**, 8855 (1988).
[2] Y. Kajikawa, J. Appl. Phys. **86**, 5663 (1999); **88**, 3784 (2000).
[3] Y. Kajikawa, Jpn. J. Appl. Phys., Suppl. **32-1**, 166 (1993).
[4] Y. Kajikawa, M. Hata, T. Isu, and Y. Katayama, Surf. Sci. **267**, 501 (1992).
[5] R. H. Henderson, D. Sun, and E. Towe, Surf. Sci. **327**, L521 (1995).
[6] Y. Kajikawa, O. Brandt, K. Kanamoto, and N. Tsukada, J. Cryst. Growth **150**, 431 (1995).
[7] Y. Kajikawa, Phys. Rev. B **51**, 16 790 (1995).
[8] Y. Kajikawa, Jpn. J. Appl. Phys., Part 1 **41**, 982 (2002).
[9] Y. Kajikawa and M. Hata, Superlattices Microstruct. **12**, 355 (1992).
[10] Y. Kajikawa, Phys. Rev. B **49**, 8136 (1994).
[11] Y. Kajikawa, Phys. Rev. B **47**, 3649 (1993).
[12] M. P. Houng, Y. C. Chang, and W. I. Wang, J. Appl. Phys. **64**, 4609 (1988).
[13] J. B. Xia, Phys. Rev. B **43**, 9856 (1991).
[14] A. T. Meney, Superlattices Microstruct. **11**, 31 (1992).
[15] Z. Ikonic, V. Milanovic, and D. Tjapkin, Phys. Rev. B **46**, 4285 (1992).
[16] T. Ohtoshi, T. Kuroda, A. Niwa, and S. Tsuji, Appl. Phys. Lett. **65**, 1886 (1994).
[17] A. Niwa, T. Ohtoshi, and T. Kuroda, IEEE J. Sel. Top. Quantum Electron. **1**, 211 (1995).
[18] G. Fishman, Phys. Rev. B **52**, 11 132 (1995).
[19] J. Los, A. Fasolino, and A. Catellani, Phys. Rev. B **53**, 4630 (1996).
[20] R. Winkler and A. I. Nesvizhskii, Phys. Rev. B **53**, 9984 (1996).
[21] G. Shechter, L. D. Shvartsman, and J. E. Golub, J. Appl. Phys. **78**, 288 (1995).
[22] G. Shechter, L. D. Shvartsman, and J. E. Golub, Phys. Rev. B **51**, 10 857 (1995).
[23] E. C. Valadares, Phys. Rev. B **46**, 3935 (1992).
[24] R. K. Hayden, E. C. Valadares, M. Henini, L. Eaves, D. K. Maude, and J. C. Portal, Phys. Rev. B **46**, 15 586 (1992).
[25] R. K. Hayden, T. Takamatsu, N. Miura, M. Henini, L. Eaves, and G. Hill, Semicond. Sci. Technol. **11**, 1424 (1996).
[26] G. Shechter and L. D. Shvartsman, Phys. Rev. B **58**, 3941 (1998).
[27] B. Laikhtman, R. A. Kiehl, and D. J. Frank, J. Appl. Phys. **70**, 1531 (1991); **70**, 5719 (1991).
[28] B. K. Ridley, J. Appl. Phys. **68**, 4667 (1990).
[29] Y. Jiang, M. C. Teich, and W. I. Wang, Appl. Phys. Lett. **57**, 2922 (1990).
[30] B. A. Foreman, Phys. Rev. B **49**, 1757 (1994).
[31] S. N. Takeda, N. Higashi, and H. Daimon, in Proceedings of the 15th International Conference on Electronic Properties of Two-Dimensional Systems (EP2DS-15), Nara, Japan 2003 (unpublished).
[32] S. S. Nedorezov, Fiz. Tverd. Tela (Leningrad) **12**, 2269 (1970) [Sov. Phys. Solid State **12**, 1814 (1971)].
[33] J. C. Phillips, *Bonds and Bands in Semiconductors* (Academic, New York, 1973).